Internal Bone Architecture in the Zygoma of Human and *Pan*

LESLIE PRYOR MCINTOSH,[1]* DAVID S. STRAIT,[2] JUSTIN A. LEDOGAR,[3] AMANDA L. SMITH,[2] CALLUM F. ROSS,[4] QIAN WANG,[5] LYNNE A. OPPERMAN,[5] AND PAUL C. DECHOW[5]

[1]School of Science and Mathematics, Abraham Baldwin Agricultural College, Tifton, Georgia 31793

[2]Department of Anthropology, Washington University in St. Louis, St. Louis, Missouri 63130

[3]Zoology Division, School of Environmental and Rural Science, University of New England, Armidale, New South Wales 2351, Australia

[4]Department of Organismal Biology & Anatomy, University of Chicago, 1027 East 57th Street, Chicago, Illinois 60637

[5]Department of Biomedical Sciences, Texas A & M University College of Dentistry, Dallas, Texas 75204

ABSTRACT

The internal and external anatomy of the primate zygoma is central to orofacial function, health, and disease. The importance of variation in its gross morphology across extinct and extant primate forms has been established using finite element analysis, but its internal structure has yet to be explored. In this study, μCT is used to characterize trabecular bone morphometry in two separate regions of the zygoma of humans and *Pan*. Trabecular anisotropy and orientation are compared with strain orientations observed in trabecular regions of finite element models of four *Pan* crania. The results of this study show that trabecular bone morphometry, anisotropy, and orientation are highly compatible with strain orientation and magnitude in the finite element models. Trabecular bone in the zygoma is largely orthotropic (with bone orientation differing in three mutually orthogonal directions), with its primary orientation lying in the mediolateral direction. Trabecular bone in the zygomatic region appears to be highly influenced by the local strain environment, and thus may be closely linked to orofacial function. Anat Rec, 299:1704–1717, 2016. © 2016 Wiley Periodicals, Inc.

Key words: trabecular bone; function; evolution; zygoma; μCT

INTRODUCTION

The primate zygomatic bone is highly variable in its shape and robusticity. One example of this variation is found in fossil specimens of contemporaneous species of australopithecines and early *Homo*. Gracile australopithecines are characterized by wider zygomas than early *Homo*, potentially a reflection of differences in dietary ecology (Strait et al., 2009; Carrier and Morgan, 2015). In the robust australopithecine *Paranthropus boisei*, it is hypothesized that the anteriorly placed zygomatic root is mechanically adapted to produce high bite force (Smith, 2015b). The variability observed in this region likely

Grant sponsors: National Science Foundation Physical Anthropology HOMINID Program; Grant numbers: NSF BCS 0725219, 0725183, 0725147, 0725141, 0725136, 0725126, 0725122, 0725078; Grant sponsor: NIH-NCRR; Grant number: P51 RR013986; NIH Base; Grant number: RR00165.

*Correspondence to: Leslie Pryor McIntosh, School of Sciences and Mathematics, Abraham Baldwin Agricultural College, 2802 Moore Hwy, Tifton, GA. E-mail: lpryor@abac.edu

Received 26 February 2016; Revised 7 August 2016; Accepted 16 August 2016.

DOI 10.1002/ar.23499

Published online in Wiley Online Library (wileyonlinelibrary.com).

hinges on its major role in orofacial function; it is located at a crucial junction between the zygomatic arch, orbital wall, and tooth bearing snout. The zygoma functions as a load bearing bone that resists and transmits masseter muscle forces from the zygomatic arch, temporalis muscle forces from the postorbital bar, and bite forces from the tooth row during a wide range of feeding behaviors, including incision and mastication. The most superior projection of the primate zygoma forms the lower part of the post-orbital bar, which expands into a postorbital septum in all anthropoid primates. As part of the lateral orbital wall, the bar and septum insulate the orbital contents from movements originating in the temporal fossa during temporalis muscle contraction and provide attachment for jaw muscles (Cartmill, 1970; Ross, 1995; Ross and Hylander, 1996; Ross and Wall, 2000).

In addition to benefiting our knowledge of craniofacial form, function and development for living humans, characterizing the gross and microscopic anatomy of this region is vital to interpreting the diversity of zygoma morphology in the primate fossil record.

Gross structural variation in the primate zygoma has been investigated using the engineering method finite element analysis (FEA). FEA is used to predict stress and strain in complex objects. It has been performed on human, chimpanzee and macaque crania, as well as fossil crania, including *Australopithecus africanus, Paranthropus boisei*, and *Australopithecus sediba* (Richmond et al., 2005; Kupczik et al., 2007, 2009; Strait et al., 2007, 2009, 2010; Chalk et al., 2011; Groning et al., 2011; Ross et al., 2011; Wang et al., 2012; Dzialo et al., 2014; Smith et al., 2015a, 2015b; Ledogar et al., 2016). The robust zygomaticoalveolar region characterizing australopithecine crania was initially hypothesized to serve as a pillar of support during the mastication of hard food objects (Rak, 1983). Rak (1983) also hypothesized that the lateral orbital wall was adapted to endure tensile strain induced by temporalis and masseter muscle usage, as in *Homo* and *Gorilla* (Endo, 1966, 1970, 1973). FE modeling of a macaque cranium demonstrated a high concentration of compressive and tensile strain in the anterior root of the zygomatic arch, medial to the masseter muscle and largely lateral to the tooth row. The vertical components of masseter muscle forces and bite force subject the zygoma to shear stress, as suggested by high tensile and compressive strains in the anterior root of the zygoma (Ross et al., 2011). On the basis of the high strains, the zygomatic bone may manifest significant adaptations to resist bone stress and strain because bone is weakest under shear (Ross et al., 2011).

While the gross structural variation of the zygoma has been investigated, the internal aspect of the region, the subcortical, or trabecular bone, has yet to be described. Assessing the characteristics and variation of trabecular bone structure and the orientation of trabeculae in the primate zygoma will aid in the interpretation of the functional and adaptive significance of the zygoma. Trabecular orientation in the post-cranial skeleton is highly correlated with tensile and compressive strain orientations. Furthermore, regions with greater trabecular density correspond to regions that experience greater stress (Lanyon, 1973, 1974; Biewener et al., 1996; Pontzer et al., 2006). Micro-computed tomography is a highly useful method of characterizing trabecular bone architecture and has been used extensively in the study of primate post-cranial bone (Hildebrand et al., 1999; Fajardo and Muller, 2001; Ryan and Ketcham, 2002a, 2002c; Ryan and van Rietbergen, 2005; Maga et al., 2006; Ryan and Krovitz, 2006; Fajardo et al., 2007; Cotter et al., 2009; Griffin et al., 2010; Ryan and Walker, 2010; Ryan and Shaw, 2012) and mandibular bone (Giesen et al., 2001; Giesen et al., 2004; van Ruijven et al., 2005; Ryan et al., 2010a).

In addition to the interpretive value that the characterization of the subcortical region of the primate zygoma will have on our understanding of the bone's role in hominid adaption and evolution, it may also benefit finite element modeling of the region. The morphological complexity of trabecular bone and the lack of tissue modulus data for primate craniofacial trabecular bone has made the modeling of trabecular bone in FEMs difficult. Therefore, zygomatic regions of primate craniofacial FEMs are modeled as solid regions using isotropic elastic properties ($E = 637$ GPa, $v = 0.28$) obtained from trabecular bone within the human tibia (Ashman et al., 1989; Strait et al., 2009). We know that the precision of FE modeling is improved when region-specific orthotropic elastic properties obtained from cortical bone are used (Dechow and Hylander, 2000; Richmond et al., 2005; Strait et al., 2005), and this is likely also the case for trabecular bone elastic properties. Possible variation between primate species and regions of the craniofacial skeleton should not be ignored.

The first aim of this study is to collect data on the density and architectural properties of trabecular bone in the zygomatic region of *Pan* and humans. Characterizing the density and the primary orientation of trabeculae is a critical first step in determining the on-axis elastic properties (those measured along the principle axis of orientation) of trabecular bone that could be used in future finite element modeling. In this study we describe the density of the whole zygomatic region (cortical plus trabecular bone), and trabecular bone density, architecture and fabric anisotropy in the zygoma of humans and *Pan* using micro-computed tomography. We compare bone volume fraction (BVF), trabecular separation, thickness and degree of anisotropy (DA), along with primary orientations of trabeculae between two human zygomatic regions (intraspecific) and between one human and the corresponding *Pan* zygomatic region (interspecific). A second aim of this study is to examine relationships between primary trabecular orientation determined by μCT analysis and patterns of strain in the zygoma of four *Pan* FEMs (Smith et al., 2015a). We expect to find that trabecular bone in the anterior root of the zygoma, which undergoes high shear strain, will be denser and have higher anisotropy than trabecular bone in the lower postorbital wall.

We hypothesize that if the zygoma is adapted to orofacial function, trabecular orientation will match primary and secondary strain orientations in the *Pan* FEMs. The gracile human craniofacial skeleton is likely adapted to processing softer foods than *Pan*, possessing smaller muscles of mastication, and also differs systemically, being characterized by relatively low bone volume fraction (Lieberman, 2011; Chirchir et al., 2015). We hypothesize that trabecular bone morphometry in the human zygoma will reflect these differences in diet, muscle morphology, and cranial robusticity found between humans and *Pan*. More specifically, we expect to find that

trabecular bone in the zygoma of *Pan* will reflect greater systemic cranial robusticity and greater muscle forces, having higher bone volume fraction, greater trabecular thickness, and greater anisotropy.

MATERIALS AND METHODS

In this study we analyze trabecular bone in humans and their closest living relatives *Pan*. Comparing trabecular bone in the zygoma of *Pan* and human may give us some insight into the differences that existed between humans and fossil hominids, as many fossil hominids share cranial features with both humans and *Pan* (Lieberman, 2011). Bony zygoma regions, extending from the lower zygomatic part of the postorbital wall, inferior to the zygomaxillary suture, to the lower border of the zygoma region (Fig. 1), were obtained from 10 human (2 females, 8 males, mean age ± SD: 54.4 ± 19.63), 4 *Pan troglodytes* (2 adult females and 2 adult males), and 1 *Pan paniscus* (adult female) crania using a Stryker bone saw and stored in equal amounts of isotonic saline and 95% ethanol. Findings for the *Pan paniscus* were grouped with those of the 4 *Pan troglodytes*. Human crania were obtained from the willed body program at the University of Texas Southwestern Medical Center. *Pan* specimens were obtained from Yerkes Primate Center, the Southwest National Primate Center, and the Antwerp Zoo (the bonobo).

Specimens were scanned in the saline ethanol solution at Baylor College of Dentistry in Dallas, Texas using a Scanco Medical μCT 35 (Scanco Medical, Basserdorf, Switzerland) at a resolution of 37 μm, an energy of 70 kVp, a current of 114 μA, and an integration time of 400 ms.

Volumes of Interest

Upper and lower zygomatic trabecular volumes were analyzed in the human specimens (Fig. 1). Because lower zygomatic regions in four out of five of our *Pan* specimens contained dense cortical bone, with little to no trabecular bone, only an upper volume was analyzed (Fig. 2). The lower trabecular region consisted of the trabecular bone within the body of the zygoma. This region was demarcated inferiorly and superiorly by upper and lower boundaries of the temporal process of the zygoma. The upper region consisted of trabecular bone in the lower post orbital bar, inferior to the zygomaticofrontal suture. The lower boundary was the lower corner of the orbit and the upper boundary was the mid-point of the post orbital wall. Trabecular bone regions were bounded posteriorly and anteriorly by the bony cortical wall of the zygoma.

All trabecular bone lying within each volume of interest (VOI) was analyzed. In Table 1, we provide the average body mass (Smith and Jungers, 1997) and trabecular bone volume that was analyzed for each species. A side by side comparison of body mass to trabecular VOI is helpful as others have found that VOIs are most accurate when scaled to body size (Fajardo and Muller, 2001). In this study, we could not scale our VOIs to body size because trabecular regions are small and irregular. However, including all the trabecular bone within the region acts as an alternative method to scaling, as these regions are then determined by the individual's morphology and indirectly, body mass (Ryan et al, 2010a; Lublinsky, 2007). Within each volume, regions of trabecular bone were contoured by hand on every 10th slice (37 μm in width). An analysis function was used to morph this contour between every 10th slice. An automatic contouring function was then applied to the existing contour to create a systematic result, by setting an inner and outer (inside the contour and outside the contour) value of mg of hydroxyapatite (HA) per cubic centimeter for the new contour to iterate. Once the values are set, the Scanco Medical contouring function will estimate the boundary between trabecular and cortical bone. Each automatic contour was inspected for accuracy. If there was an error in the contour, it was altered manually.

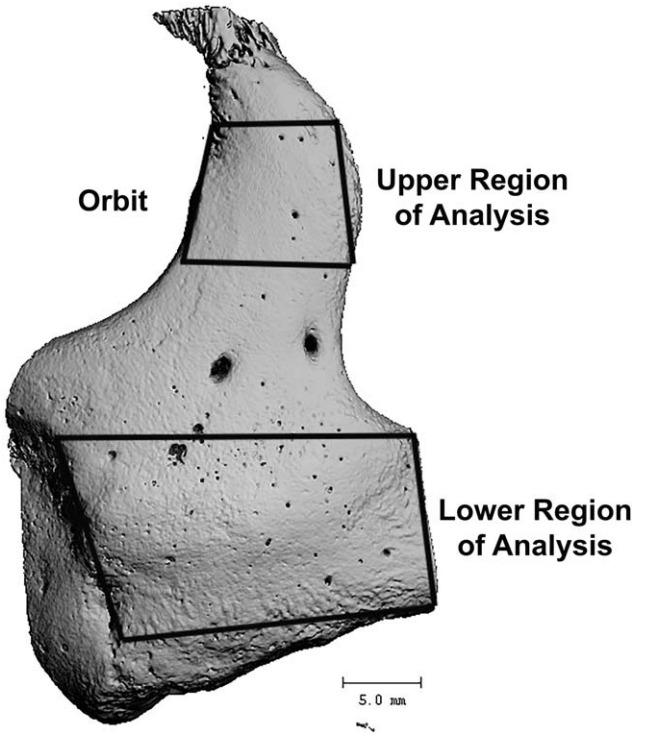

Fig. 1. Human zygomatic bone rendered from a microCT scan showing upper and lower regions of analysis.

Segmentation

The Ridler and Calvard (1978) and Trussell (1979; Ryan and Ketcham, 2002c; Ryan and Ketcham, 2002b) method, provided by Scanco Medical as an image processing language script (IPL), was used to extract the mineralized bone phase. The threshold for each specimen was therefore individualized (Table 2). A μCT technician at Baylor College of Dentistry conducts weekly scans using a phantom bone specimen to calibrate density values for the machine.

Micro-CT Analysis of Whole and Trabecular-Only Zygomatic Regions

Bone volume fraction (BVF; marching cubes method), and material and apparent density were determined for

TABLE 1. Body mass and volumes of interest

	N			Estimated Body Weight (kg)		Trabecular Upper Zygoma VOI volume (mm^3)		Trabecular Lower Zygoma VOI volume (mm^3)	
Species	m	fm		m	fm	m	fm	m	fm
Homo sapiens	8	2	Mean	72.1	62.1	257	341	993	1657
			SD	11.4	9.88	191	151	625	427
Pan troglodyte	1	3	Mean	60	47.4	107	63		
			SD	ua	ua	-	36		
Pan paniscus		1	Mean	45.0	33.2	-	79		
			SD	8.4	4.2	-	-		

Estimated body weight means and S.D. in kg and trabecular bone volumes in mm^3 are presented by species and number of sample (n) for both male (m) and female (fm) (Smith and Jungers, 1997). "ua" values were unavailable. "-" values were not measured.

TABLE 2. Individualized thresholds

Specimen	Threshold (HU)
Human 992	478.2
Human 1087	496.1
Human 1095	336.9
Human 1099	472.8
Human 1103	552.5
Human 1107	444.8
Human 1111	502.6
Human 1115	405.4
Human 1119	561.4
Pan 1037	447.3
Pan 2845	539.4
Pan 2849	544.1
Pan 2933	540.7
Pan 3990	478.8

Thresholds in Hounsfield Units (HU) as determined by the Ridler and Calvard (1979) and Trussell (1979) method are reported here for all 5 *Pan* and 10 *Homo* specimens.

whole bone regions (including cortical shell and trabecular bone; based on gray values defined by a phantom specimen) (Lorensen and Cline, 1987). Apparent density describes the milligrams of hydroxyapatite per cubic centimeter that include bone material and voids. The material density describes the milligrams of hydroxyapatite per cubic centimeter of the bone material excluding all voids, or non-bone material.

Once contoured and thresholded, a pre-written IPL script (Scanco Medical software) was applied to determine degree of anisotropy (mean intercept length method), and structure model index (triangulation method) which are described in more detail below. Trabecular separation, thickness, and number [distance transformation method (Hildebrand and Rüegsegger, 1997; Hildebrand et al., 1999)] connectivity density [Euler method (Odgaard and Gundersen, 1993)], and bone volume fraction (BVF) are also provided by the prewritten script. Degree of anisotropy (DA) is a unit-less description of how oriented the bone material is. The mean intercept length method projects lines across the volume of interest and measures the distances between the bone and void interfaces (Whitehouse, 1974; Harrigan and Mann, 1984). It then averages these distances to determine the amount of bone aligned in that direction. The direction with the greatest amount of bone material is the primary orientation and is provided as an eigenvector with a magnitude that is described by the Scanco Medical system as "H2". It then projects lines in the mutually orthogonal directions to measure the distance between bone and void interfaces. The direction with the next to least amount of bone is the eigenvector "H3" and the direction with the least amount of bone is the eigenvector "H1". In addition to providing the relative magnitude, as described by the number of the eigenvector, Scanco Medical provides the coordinates of the eigenvector so that directionality can be determined. The DA is a ratio of the magnitude of H2 to H1 or the amount of bone in the direction of primary orientation to the tertiary direction. Terms used to describe types of cortical and trabecular bone anisotropy include isotropy (where bone material is the same in three mutually orthogonal directions), orthotropy (where bone material differs in three mutually orthogonal directions), and transverse isotropy (where bone material is the same in two of the three mutually orthogonal directions, but differs in the third). As calculated by the Scanco Medical bone morphometric script, a low DA (close to 1), implies that the bone is isotropic, whereas an increasing DA (greater than 1), implies increasing orthotropy or transverse isotropy. In this study, DA (H2:H1) is provided, but the ratio of eigenvector magnitudes H2 to H1 and H3 to H1 are also calculated to better characterize the type of anisotropy in the region.

Structure model index (SMI) is a unit-less measure of the "type" of trabecular bone (Hildebrand and Rüegsegger, 1997; Hildebrand et al., 1999). The type of trabecular bone can be described as rod-like, plate-like, or honeycomb-like. An SMI at or nearing 3 is more rod-like whereas an SMI at or nearing 1 is more plate-like. A negative SMI describes trabecular bone that is very dense and honeycomb-like, and might even be described as highly porous cortical bone. Measures of the thickness and separation of trabeculae are averaged from the volume of interest and measured in cubic millimeters, whereas trabecular number measures the number of trabeculae per cubic millimeter. The connectivity density describes the concentrations of connections between trabeculae in cubic millimeters.

Statistical Analysis

Significant differences in measures of trabecular morphology by region between each species were determined

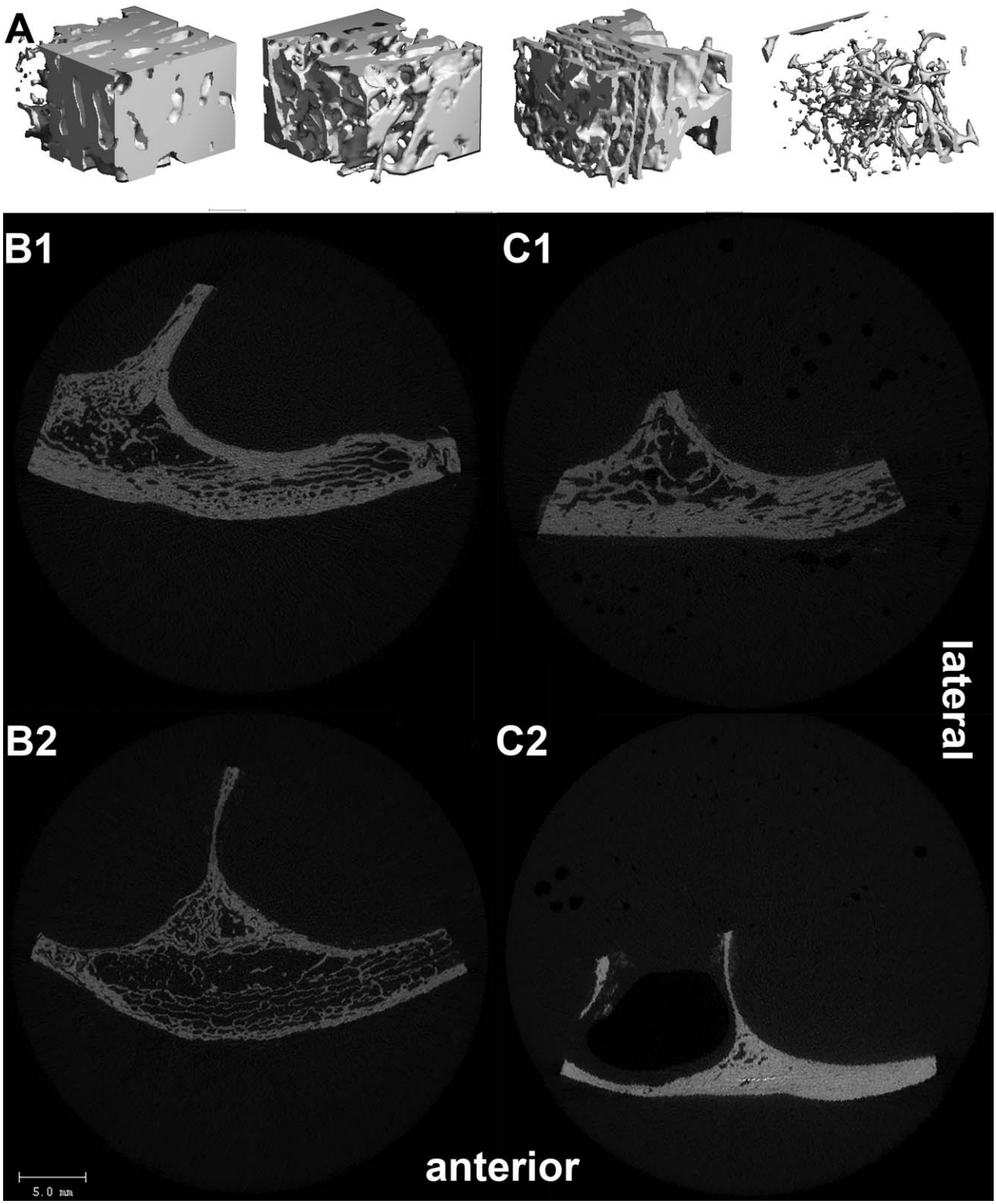

Fig. 2. **A**: Rectangular regions measuring approximately 25 mm^2 and 10-mm thick of trabecular bone rendered from human lower zygomatic body regions, showing individual and intraspecific variability in trabecular structure throughout this region. **B**: Transverse section of a μCT scan of a human zygomatic body (1, 2) showing plate-like trabecular structure in the lateral end transitioning to more sparse rod-like trabecular bone in the medial region. **C**: Transverse section of μCT scan of two *Pan* specimens, with (C1) trabecular bone and without (C2). Specimens were scanned in a saline alcohol solution; the darker spots in (C1) and (C2), including the large black area in (C2) represent air pockets that were trapped in the sample tube.

TABLE 3. Zygomatic density of whole bone

Species	Location	BVF[a] Mean	BVF[a] S.D.	Apparent density (mg HA/cm^3) Mean	Apparent density (mg HA/cm^3) S.D.	Material density (mg HA/cm^3) Mean	Material density (mg HA/cm^3) S.D.
Homo	**Upper Zygoma**	0.83	0.08	819	77	979	27
Pan	**Upper Zygoma**	0.93	0.04	898	69	966	47

Bone volume fraction (BVF; to the nearest hundredth), and apparent and material density (to the nearest mg of hydroxyapatite per cubic centimeter) for whole bone (cortical + trabecular bone) upper zygomatic regions.
[a]BVF is significantly different between *Pan* and *Homo*.

by Mann-Whitney U tests (IBM SPSS Statistics Version 22, Armonk, NY). Intraspecific differences between the two human regions were explored using the Wilcoxon sign test (SPSS). Primary, secondary, and tertiary eigenvectors (H2, H3, and H1, respectively) were plotted relative to basic Frankfurt horizontal anatomical axes using OriginLab Pro (OriginLab, Northhampton, MA). Oriana (Kovach Computing Services, Pentraeth, Wales, UK) was used to calculate mean angle and standard deviations for each eigenvector. Significance of each mean angle was tested using Rayleigh's test (performed in Oriana) for uniformity and intra and interspecific significant differences were tested using the Watson-Williams F test for multiple comparisons ($P \leq 0.05$) (performed in SPSS) Wang and Dechow, 2006; Zar, 1999).

Finite Element Analysis of the *Pan* Zygoma

This study utilized 4 *Pan* cranial FEMs and their corresponding analyses to capture the internal strain patterns in the zygoma during orofacial function, describing primary, secondary, and tertiary strain (Smith et al., 2015a). The FE models were built from 4 CT scans representing the morphological extremes of a collection of 19 *Pan* cranial specimens. The models incorporated region-specific values of cortical bone properties and muscle force for the anterior temporalis, deep and superficial heads of the masseter and the medial pterygoid (Strait et al., 2009; Smith et al., 2015a). The cortical bone elastic values were all acquired using ultrasound from one of the female *Pan* specimens (See Smith et al., 2015a) used in the morphometric analysis of this study (different from the *Pan* CT scans that were used to create the FEMs) and reported, along with the mechanical properties of the remaining four *Pan* crania (making a total of five *Pan* crania), by Gharpure et al. (in press) in this issue of the Anatomical Record. Trabecular regions were represented as solid separate objects. Isotropic tissue modulus values obtained from human tibial trabecular bone were assigned to these objects (Ashman et al., 1989). Finite element analysis was performed on each model by Smith et al. (2015a), with constraints at both left and right temporomandibular joints. Bite point forces were applied at the third premolar and the second molar. For this study, in order to describe the strain orientations in the trabecular region of the FEA results, the cortical bone was hidden revealing the trabecular objects and their strain vectors [See Smith et al. (2015a)]. In the results section, primary, secondary and tertiary strain orientations and relative magnitudes from these FE models are described and discussed relative to our μCT determinations for trabecular orientations and bone density.

RESULTS

μCT Analysis of the Zygoma

This study analyzed two regions of the zygoma, including an upper region, contained in the lower post-orbital bar above the level of the anterior root of the zygomatic arch, and a lower region, lying directly medial to the anterior root of the zygomatic arch. Differences in trabecular bone type and volumes were visible in most individuals of the human sample across the zygomatic body and between humans and *Pan*. Figure 2A demonstrates the variation in trabecular structure found among our human sample in the zygomatic body and includes trabecular bone from the same individual and from different individuals (which lies adjacent to the temporal process of the zygomatic bone). One human lower zygomatic bone did not contain trabecular bone and was not analyzed. Furthermore, trabecular bone type appeared to differ across the human zygomatic body from lateral to medial, such that plate-like trabecular bone tends to lie parallel to the cortical surface in the lateral region of the zygomatic body, but tends to thin out and become more rod-like in the medial region of the zygomatic body. Figure 2B1,B2 not only show the relatively large region of trabecular bone found within the zygomatic body in two of our human specimens, but demonstrate this pattern of trabeculae. Despite this obvious medio-lateral variation, we performed our morphometric analyses on the zygomatic body as a whole because objective demarcation of medial from lateral regions was not possible. Instead, we noted what might be major differences in strain across the zygomatic body associated with these differences in trabecular bone type and orientation.

Additionally, large differences between the zygomatic body (lower region) between our human and *Pan* samples were observed. Lower zygomatic regions in *Pan* were for all but one specimen nearly filled in with dense bone, leaving no discernable trabecular region for analysis. Figure 2C1 is a cross section of the one *Pan* individual that contained trabecular bone within the body of the zygoma. Figure 2C2 is a cross section of the body of a *Pan* zygoma that is representative of the remainder of the sample. Both human and *Pan* samples contained discernable trabecular bone regions in the upper zygoma/lower post-orbital bar.

TABLE 4. Trabecular bone morphometry

Species	Site	BVF M	BVF S.D.	DA M	DA S.D.	Tb.N (mm^3) M	Tb.N (mm^3) S.D.	Tb.Th (mm^3) M	Tb.Th (mm^3) S.D.	Tb.Sep (mm^3) M	Tb.Sep (mm^3) S.D.	SMI M	SMI S.D.	ConnD (mm^3) M	ConnD (mm^3) S.D.	MD (mg HA/cm^3) M	MD (mg HA/cm^3) S.D.
Homo	**L**	0.30	0.10	1.87	0.37	1.46	0.34	0.28	0.06	0.72	0.19	1.25	1.03	4.86	1.83	842	40.2
	U	0.36	0.13	1.39	0.23	1.43	0.37	0.30	0.08	0.72	0.24	1.08	0.73	15.75	8.80	886	59.7
Pan	**U**	0.62	0.12	1.75	0.43	2.11	0.25	0.37	0.08	0.45	0.11	0.22	0.67	14.26	6.39	906	48.8
Homo vs Pan	**U**		*0.005*		0.099		0.055		0.679		*0.005*		0.055		*0.013*		0.594
Homo	**U vs. L**		0.14		*0.015*		0.77		*0.021*		0.77		0.374		0.95		*0.015*

Mean (M) and standard deviation (S.D.) of trabecular bone descriptors (rounded to the nearest hundredth) determined by μCT trabecular bone analysis for upper (U) and lower (L) zygomatic regions in humans and the upper (U) zygomatic region of *Pan*. Parameters include degree of anisotropy (DA), trabecular number (Tb.N), trabecular thickness (Tb.Th), trabecular separation (Tb. Sep), structure model index (SMI), connectivity density (ConnD) and material density (MD). Interspecific significance of trabecular bone descriptors determined by Mann-Whitney U tests performed between *Homo* and *Pan*, where $P \leq 0.05$. Intraspecific differences of trabecular bone descriptors between upper and lower zygoma regions in *Homo* determined by Wilcoxon Sign test, where $P \leq 0.05$.

Whole Bone Analysis

Before analyzing the trabecular region, we conducted analysis on both cortical and trabecular bone in the upper zygomatic region to look at differences in the overall density of the lower post-orbital region in humans and *Pan*. Density measures of combined trabecular and cortical bone regions of the upper zygoma found that BVF (ratio of bone volume to total volume) is significantly greater in *Pan* ($P = 0.008$). While apparent density (density of the bone material and voids) is greater in *Pan* and material density (density of only bone material) is greater in humans, these differences were not statistically significant (Table 3).

TRABECULAR BONE ANALYSIS

Interspecific and Intraspecific Comparisons of Trabecular Bone Morphometry

Table 4 provides means and standard deviations of trabecular bone morphometric variables in the upper and lower human and upper *Pan* zygomas. Table 4 also provides the results of the Mann-Whitney U significance tests. Upper *Pan* zygoma regions have greater BVF ($P = 0.005$) and trabecular number ($P = 0.005$), and significantly less trabecular separation ($P = 0.013$) relative to upper human zygoma regions.

Wilcoxon tests for intraspecific differences between upper and lower human zygoma regions found significant differences in degree of anisotropy ($P = 0.015$), connectivity density ($P = 0.021$), and material density ($P = 0.015$). Lower human zygoma regions were more anisotropic, but less materially dense and with lower connectivity density (Table 4).

Material Distribution and Angular Orientation

Material orientation computed by our μCT analysis is expressed by three eigenvectors: H2, which provides direction and magnitude of the primary orientation of trabecular bone material (the direction in which most bone material is oriented); H3, which provides direction and magnitude of the secondary orientation of trabecular bone material; and H1, which provides direction and magnitude of the tertiary orientation of bone material. Comparing H2 to H1 eigenvector magnitudes in each region shows that the lower zygoma is more strongly oriented, having a higher degree of anisotropy (Fig. 3A). Degree of anisotropy only measures the ratio between 2 eigenvector magnitudes, so while it can determine if the bone is anisotropic, it is inconclusive regarding the type of anisotropy (orthotropy vs. transverse isotropy). Therefore, all three eigenvector magnitudes were compared (Fig. 3B–D). Trabecular bone in the lower zygoma (human only) is more orthotropic (mean eigenvector magnitudes differ in three directions, with eigenvector magnitude ratios of 1.87, 1.52, and 1.25) than the upper zygoma which is more transversely isotropic (H2 and H3 eigenvector magnitudes are very similar, their ratio averaging 1.18) (Fig. 3). This is demonstrated in Figure 3 by observing the data points for each ratio relative to the line $y = x$.

An important distinction between regions is that in the upper zygoma, primary and secondary vectors are closer in magnitude, while in the lower zygoma, secondary and tertiary vectors are closer in magnitude. This

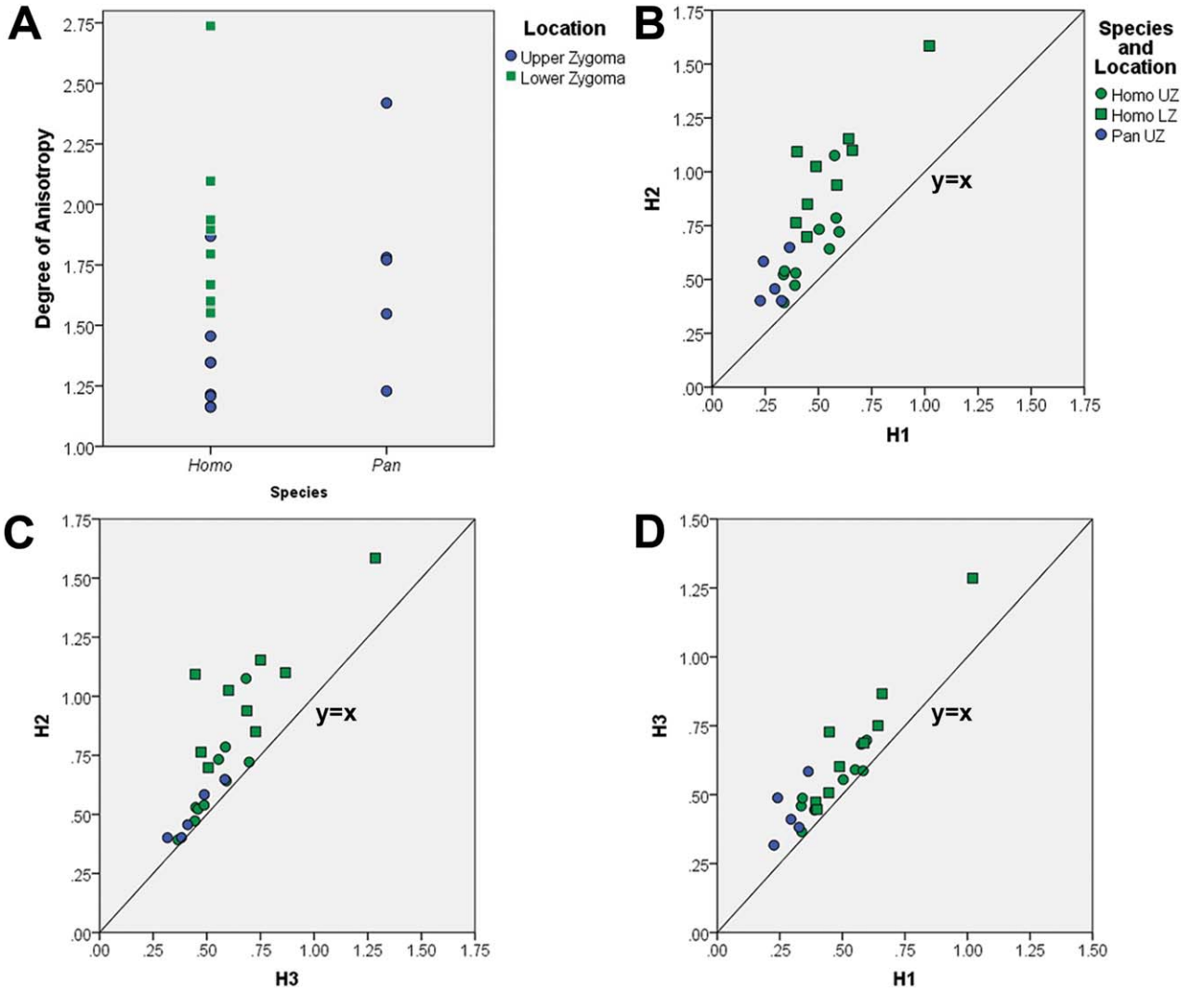

Fig. 3. **A**: Degree of anisotropy across individuals in human (upper zygoma,10 individuals; lower zygoma, 9 individuals) and *Pan* (upper zygoma, 5 individuals). When considered together, ratios between each of the three eigenvectors demonstrate the type of anisotropy (transverse isotropy, orthotropy, and isotropy). For example, if the H2 and H1 eigenvectors differ greatly, but the H2 and H3 eigenvector are very similar, the trabecular structure can be described as transversely isotropic (orientation differs in only two orthogonal directions). Ratios are demonstrated using bivariate plots of the primary vector of trabecular orientation (H2) to the tertiary (H1) vector of trabecular orientation (B), of the primary vector of trabecular orientation (H2) to the secondary (H3) vector of orientation (C), and of the secondary vector of orientation (H3) to the tertiary (H1) vector of orientation (D). For each bivariate chart, a line ($x = y$) demonstrates a one to one ratio. In other words, data points that fall on this line are those where there is no difference in magnitude between the two eigenvectors. The outlier in each bivariate plot is a human male with a higher bone volume fraction than most in the sample, which explains a greater magnitude in associated eigenvectors.

means that in the upper zygoma, bone material is more strongly oriented in two directions, while in the lower zygoma, material is oriented more strongly in one primary direction. Rayleigh's test for uniformity was used to determine significance in the orientation of eigenvectors, testing the null hypothesis that eigenvectors angles are randomly distributed. In the lower human zygomatic region, average orientation of H2 (primary) vectors, was significantly oriented ($P < 0.001$), lying in a mediolateral direction, and nearly 90 degrees from an anteroposterior (AP) and inferosuperior (IS) axes (Table 5; Fig. 4). In the human upper zygomatic region, average orientation of H2 was around 90 degrees away from the AP axis ($P < 0.001$), while in the *Pan* upper zygomatic region, average H2 was significantly oriented 72 degrees away from the IS axis ($P < 0.01$). Average secondary (H3) orientation in the lower human zygoma varied only in the sagittal plane, being significantly oriented 89 degrees from the mediolateral direction ($P < 0.001$). In the upper zygomatic region of humans and *Pan*, secondary orientations varied in their orientation only in the transverse plane. Tertiary (H1) eigenvectors in lower and upper human and upper *Pan* regions were significantly oriented between 90 and 100 degrees away from the mediolateral direction ($P < 0.001$), varying greatly in orientation in sagittal plane (Table 5; Fig. 4). Both upper zygoma

TABLE 5. Orientation of trabeculae

Species	Site	Mean	S.D	*P*	Mean	S.D	*P*	Mean	S.D	*P*
Primary		H2-Inferosuperior Axis			H2-Anteroposterior Axis			H2-Mediolateral Axis		
Homo	**L**	92	11	*<0.001*	87	11	*<0.001*	0	16	<0.001
	U	51	35	0.081	94	13	*<0.001*	134	61	0.890
Pan	**U**	72	14	*0.01*	154	41	0.56	76	31	0.220
Secondary		H3-Inferosuperior Axis			H3-Anteroposterior Axis			H3-Mediolateral Axis		
Homo	**L**	122	48	0.62	139	38	0.274	89	10	*<0.001*
	U	106	29	*0.018*	101	50	0.585	110	40	0.22
Pan	**U**	99	9	*0.003*	88	33	0.290	177	38	0.45
Tertiary		H1-Inferosuperior Axis			H1-Anteroposterior Axis			H1-Mediolateral Axis		
Homo	**L**	36	38	0.263	64	42	0.39	92	12	*<0.001*
	U	78	41	0.232	28	60	0.85	90	23	*0.001*
Pan	**U**	21	5	*0.002*	89	18	*0.026*	99	7	*0.002*

Mean angle orientations and standard deviations rounded to the nearest degree and Raleigh Test of significance *P* value of the primary eigenvector H2, secondary eigenvector H3, and tertiary eigenvector H1 from inferosuperior, anteroposterior, and mediolateral axes in *Homo* and *Pan* upper (U) and lower (L) zygomatic regions ($P \leq 0.005$).

human and *Pan* H3 orientations were significantly oriented nearly 90 degrees from the mediolateral axis and H3 was significantly oriented 106 and 99 degrees, respectively, from the inferosuperior axis.

Watson-Williams F tests detected a significant difference in angular orientation between upper zygomatic regions of human and *Pan* for H2 ($P = 0.003$) and H1 ($P < 0.001$). Significant differences were found in H2 ($P < 0.001$) and H1 ($P = 0.02$) orientations between upper and lower human zygomatic regions.

Finite Element Modeling of the Internal Zygoma of *Pan*

Overall patterning of strain orientation in the working side zygoma of the *Pan* finite element models did not differ much between individuals or between PM3 and M2 biting. In the zygomatic body of the *Pan* finite element models, there appears to be two patterns of primary and secondary strain orientation on the biting side, differing laterally to medially. More laterally, near the temporal process of the zygomatic bone, primary and secondary strain tensors fall in a transverse plane. The primary tensor (tension) lies in the mediolateral orientation with a slight anteroposterior tilt. The secondary tensor (compression) lies mediolaterally, with a superior tilt at its lateral end (Fig. 5). Towards the medial border of the zygomatic body, the primary tensor (tension) lies mediolaterally, while the secondary tensor (compression) lies superoinferiorly.

In the upper zygomatic region, both primary (Fig. 5A) and secondary (Fig. 5B) strain tensors undergo large changes in orientation moving inferosuperiorly. At the lower end, tension is directed along an inferosuperior axis and gradually changes to an inferomedial-superolateral orientation. Compression is found along a mediolateral axis in the lower end of this region and it gradually shifts to an inferolateral-superomedial direction (nearly superoinferior). Additionally, vectors in this region are much smaller in magnitude compared to the zygomatic body (Fig. 5).

DISCUSSION

In this study, we used micro-computed tomography to characterize cortical and trabecular bone density, architecture and fabric anisotropy in the zygoma of humans and *Pan*. We hypothesized that trabecular bone in the anterior root of the zygoma (lower zygomatic region of our analysis), which undergoes high shear strain, will be denser and have higher anisotropy than trabecular bone in the lower postorbital wall (upper zygomatic region of our analysis). Our results only partially support this hypothesis. Trabecular bone in the anterior root of the zygoma (lower zygoma region) is significantly more anisotropic than trabecular bone in the lower post-orbital bar. Trabecular bone in the human upper zygoma/lower post-orbital bar was significantly more materially dense (higher mg HA/cm^3) and had significantly greater connectivity density compared to trabecular bone in the lower zygomatic region of humans. However, our qualitative findings suggest that in our chimp sample, lower zygomatic regions are denser overall than upper regions, containing virtually no trabecular bone in all but one *Pan*.

Additionally, we hypothesized that if the zygoma is functionally adapted to orofacial function, trabecular orientation, especially in our *Pan* specimens, should match primary and secondary strain orientations in the *Pan* FEMs. The results of this study are consistent with this hypothesis, finding that trabecular bone alignment is significantly oriented in a mediolateral direction, corresponding to the primary (tension) strain tensor observed across the anterior root of the zygoma in our *Pan* FEMs. In the more lateral region, primary and secondary strain tensors form a transverse plate of shear strain, while more medially, secondary strain transitions from an anteroposterior orientation to an inferosuperior

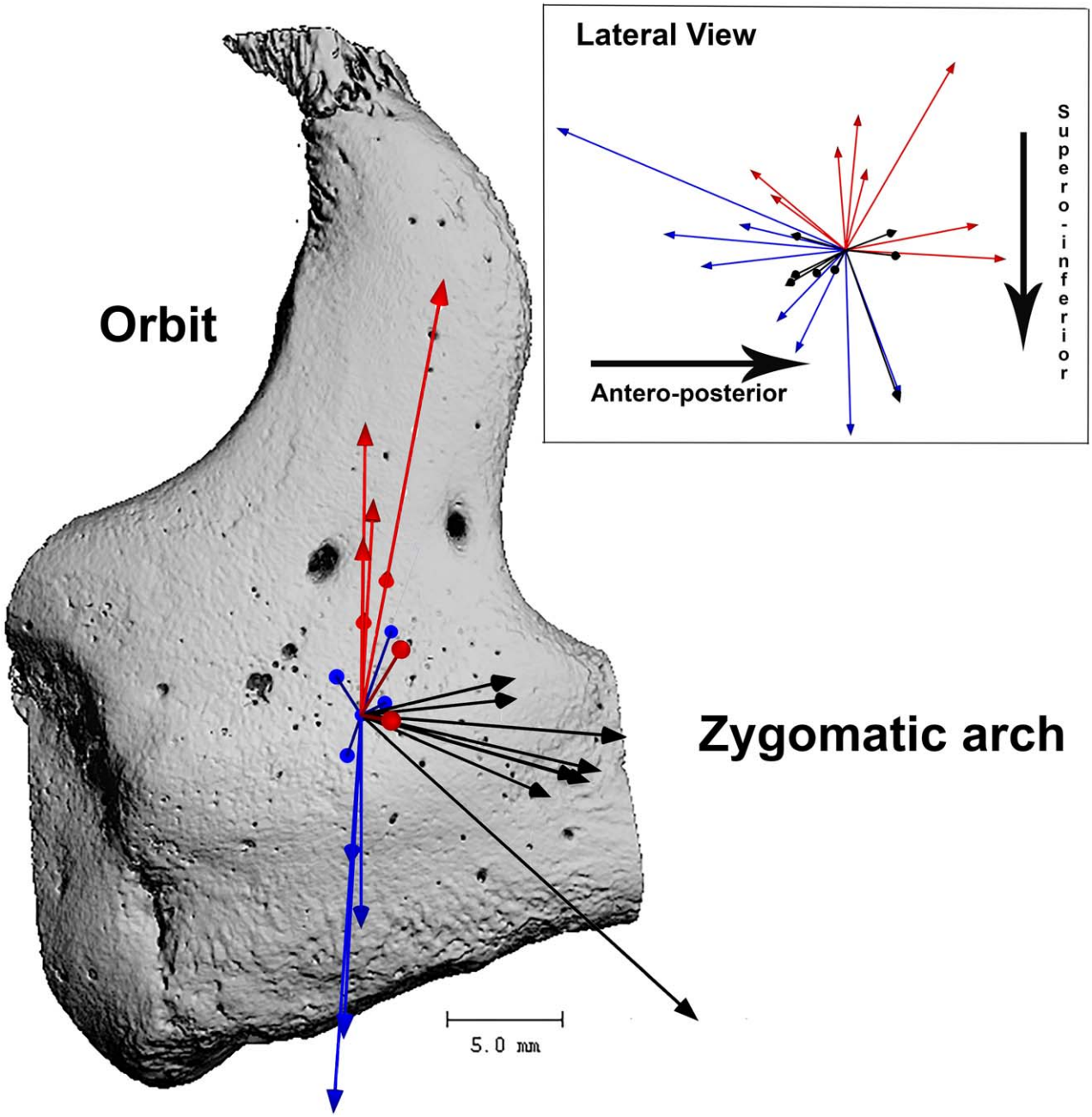

Fig. 4. Anterior view of primary (black), secondary (red), and tertiary (blue) vectors of trabecular orientation in the human lower zygoma (zygomatic body) superimposed on a μCT rendering of the human zygoma. The lateral perspective shows that secondary and tertiary eigenvectors vary in a sagittal plane, and demonstrate the consistency of primary vector in the mediolateral direction.

orientation. The average trabecular bone material orientation across the region (lateral to medial) showed greater variability in secondary and tertiary material orientation eigenvectors. This finding would be expected based on the variability observed in the secondary strain tensor in our *Pan* FEMs. Material orientation in the lower post-orbital bar/upper zygomatic region was also consistent with strain orientation patterns in our *Pan* FEMs. We found little significance in trabecular material orientation: in *Pan*, primary orientation of trabecular bone was significantly oriented relative to the inferosuperior axis, while in humans, primary trabecular orientation was significantly oriented 94 degrees from the anteroposterior axis. In our *Pan* FEMs, primary and secondary strain tensors appear to be undergoing a transition in orientation, which would predict greater variability of trabecular material orientation in this region. Furthermore, the greater anisotropy observed in the

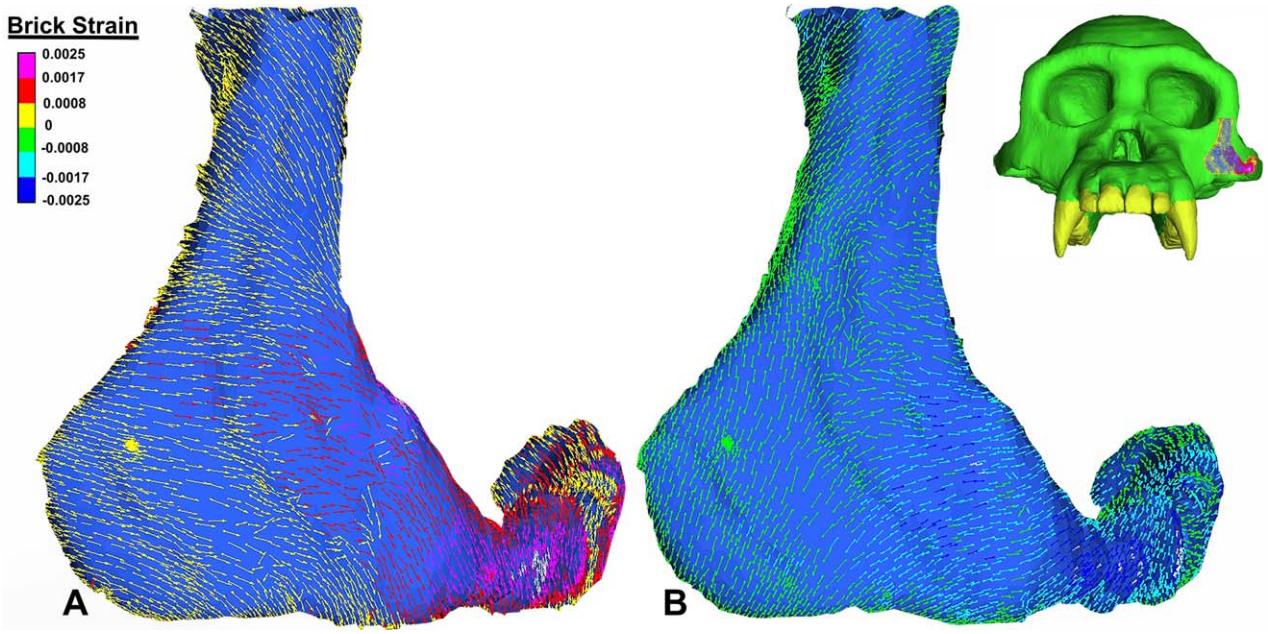

Fig. 5. **A**: Anterior view of left zygomatic trabecular region from the biting side of a *Pan* finite element model (PC1-), demonstrating primary strain (tension) in the upper and lower zygomatic regions during molar biting. Strain magnitude in the upper zygomatic or postorbital region is lower than in the lower/zygomatic body region. **B**: Anterior view of the left zygomatic trabecular region showing secondary strain (compression) in upper and lower zygomatic regions.

lower zygoma is consistent with a greater number of strain tensors with higher magnitudes of tension in this region compared to the upper zygoma.

Regarding interspecific differences in trabecular morphometry, we hypothesized that *Pan* zygomatic regions would be characterized by greater bone volume fraction, trabecular thickness, and high anisotropy. Our results support this hypothesis. We found that trabecular bone in the upper *Pan* zygoma is characterized by significantly higher bone volume fraction and trabecular thickness. Degree of anisotropy was higher in *Pan*, but this difference was not significant. The differences we observed between the lower zygomatic regions also support this hypothesis.

Currently, trabecular bone in the zygoma is being modeled as a solid region using isotropic elastic properties obtained from the human tibia ($E = 637$ GPa, $v = 0.28$) (Ashman et al., 1989). The results of the current study suggest that trabecular bone in the zygomatic region of humans and *Pan* differs drastically in bone type (as described by structure model index), density, trabecular thickness, and anisotropy compared to human tibial trabecular bone. Relative to that in the tibia, trabecular bone in the zygomatic region is more plate-like, has higher bone volume fraction, greater trabecular thickness, and lower anisotropy (Ding et al., 2003). Determining the elastic properties of trabecular bone from the zygomatic region would be challenging, but replacing these values with more realistic ones would likely improve the accuracy of finite element analysis of the primate craniofacial skeleton. Furthermore, we found that 4 out of 5 of our *Pan* specimens did not have trabecular bone volumes in the zygomatic body, while all of the *Pan* FE models used contained sizable trabecular bone regions within the zygomatic bone. Zygomatic body trabecular regions in the four *Pan* finite element models were created from CT scans of entire chimpanzee crania and are of a much lower resolution. The resolution of the CT scans may not have allowed proper determination of the size and extent of the trabecular region in the zygoma of the four *Pan* FEA crania, or this may result from intraspecific variation. The results of this study cannot provide a satisfactory answer. An important goal of future work is to determine the extent of this variability across populations of *Pan*; perhaps, in *Pan* FEMs, the lower zygomatic body would be better modeled as a thick plate of bone with no trabecular volume.

Inter and Intraspecific Differences in Trabecular Morphometry

In primate postcranial regions, trabecular BVF, thickness, and separation increase with increasing body size, but with negative allometry (Ryan and Shaw, 2013). Patterns of trabecular bone morphometry appear to be related to taxonomic order, such that Old World monkeys have relatively thick and sparse trabeculae whereas apes have a greater number of comparably thin, densely packed trabeculae. In this study, we found that some variables (BVF, trabecular number, and trabecular separation) differ significantly between species, while other variables (degree of anisotropy, connectivity density, and material density) differ significantly across anatomical locations. Consistent with previous studies, *Pan* had greater trabecular BVF, which was likely the result of a higher number of trabeculae with lower trabecular

spacing. The statistically smaller BVF found in our human sample is consistent with other human cranial (Pryor, 2015) and post-cranial (Chirchir et al., 2015) regions where trabecular bone is approximately 50%–75% the BVF of *Pan*.

Variables that were significantly different between species were not the same variables that we found to differ significantly between locations. Variables that differed significantly between human zygomatic locations included degree of anisotropy, connectivity density, and material density. This finding suggests that some morphometric variables (like BVF) are more likely systemic, while others are more influenced by the local strain environment. This observation is useful for interpreting the meaning behind such variation. For example, if BVF is more of a systemic variable, then it may not be safe to assume that the resulting increase in strength due to increasing BVF is functionally significant at that specific location. On the other hand, looking at changes in BVF of trabecular bone between regions of the same species may indicate that differences in BVF are related to function. In the case of the primate zygoma, increases in the BVF of trabecular bone regions in the lower zygoma that lead to completely dense zygomatic regions may allude to the functional need of the lower *Pan* zygoma to be stronger than the human zygoma, which has large, highly trabeculated lower zygomatic regions.

The Relationship between Bone Material Orientation and Strain in the Craniofacial Skeleton

Using finite element models of four *Pan* crania undergoing molar and premolar biting, we described primary, secondary, and tertiary strain orientations in upper and lower trabecular bone regions. We observed the following:

1. Primary and secondary strain orientations on the working side are similar across all four models.
2. On the working side lower zygomatic region near the anterior root of the zygomatic arch we observed primary (tension) and secondary (compression) strain of a high magnitude lying in a transverse plane.
3. Moving medially across the lower zygomatic region of the working side, primary and secondary strain tensors change such that primary strain is oriented in the mediolateral direction and secondary strain is oriented in the superoinferior direction and strain magnitudes decrease overall.
4. In the upper zygomatic region of the biting side, primary and secondary strain orientations are more variable. However, each lie nearly orthogonal to one another in the coronal plane, each approximately 45 degrees from the inferosuperior axis.
5. The lower zygomatic body is characterized by strain of a higher magnitude compared to the upper zygomatic region. On the whole, this region has higher primary or tensile strain tensors than secondary or compressive strain tensors.

The relatively high degree and consistent mediolateral orientation of tension across the lower zygoma would predict that this region of the zygoma should be characterized by higher anisotropy and that the primary eigenvector should lie in the mediolateral direction and be much larger than secondary and tertiary eigenvectors. The results of our μCT analysis are highly consistent with these predictions. One possible explanation for the thick cortical plate that characterized four out of five of our *Pan* specimens is that greater strain magnitudes that would be expected in *Pan* would lead to the filling in of bone in the coronal plane. Furthermore, we observed a transition in trabecular bone type moving lateral to medial in most of our human sample, such that the thick coronally oriented plates found in the more lateral region of the zygomatic body thin out and become shorter in the more medial region of the zygomatic body. Compressive strain orientations in the superoinferior direction forming in this region would predict this transition. The lack of significance in most of the angle orientations in the upper zygomatic region and the lack of consistency between human and *Pan* primary orientations would be predictable based on the variability of strain orientations in the *Pan* FEMs. Additionally, moderate and proportionate primary and secondary strain in this region predict that primary and secondary trabecular orientations would be similar in magnitude, as was observed.

Trabecular bone type in both upper and lower zygomatic regions was plate-like. Plate-like trabecular bone structure has been observed in other regions of the primate craniofacial skeleton, including the mandibular condyle and the supraorbital region (Giesen and van Eijden, 2000; Pryor, 2015). In the mandibular condyle and the supraorbital region, bony plates are oriented in the sagittal plane, whereas in the lower human zygomatic region, plates are observed in the mediolateral direction, falling in the coronal plane. Furthermore, inconsistencies between the supraorbital and lower zygomatic region are found in the variability of each eigenvector. In the lower zygomatic region, the primary eigenvector lying in the mediolateral direction is the most consistent. In the supraorbital region, the mediolateral eigenvector is also the most consistently oriented, however, it comprises the tertiary eigenvector, which describes the least amount of bony material (Pryor, 2015). In both cases, the most consistent alignment occurs near the direction of primary strain in the *Pan* FEMs. Giesen et al. (2001) hypothesize that trabecular structure in the mandibular condyle is adapted to endure low stress from multiple directions, as opposed to unidirectional loads of high magnitude as observed in the zygoma (van Ruijven et al., 2002; Giesen et al., 2004). Our findings in this paper, combined with those reported elsewhere, support this hypothesis: trabecular bone orientation and anisotropy in the zygoma differs from that observed in the condyle and the supraorbital region (Pryor, 2015).

SAMPLE AND LIMITATIONS

Our human sample contained more males than females and our chimp sample contained more females than males. We had at least three human individuals over the age of 70 (one individual's age was unknown), and one adult under the age of 40. We did not test the effects that age or sex played on the BVF of our sample (Aaron et al., 1987; Goldstein et al., 1993; Kneissel et al., 1994; Fajardo and Muller, 2001). Because of our

sample size, it was difficult to tell if the data was normally distributed. This led us to perform nonparametric statistics to decrease the likelihood of type 1 error.

Trabecular bone analysis is subject to oversampling error. Ideally, VOIs should therefore be scaled to body size (Fajardo and Muller, 2001). In this study, we were limited by small regions of trabecular bone and large interspecific variations in the amount of trabecular bone. We therefore were not able to scale regions by body size, but instead analyzed all trabecular bone within each region. While our VOIs were influenced by body size across the individual and species level (Lublinsky et al., 2007; Ryan et al., 2010a), comparison of our trabecular VOIs and mean body size found large inconsistencies. This is likely attributable to differences in morphology between humans and *Pan*: for example, *Pan* upper zygoma regions were generally shorter than upper zygoma regions in humans. Trabecular volumes in the upper zygoma are fairly small and in some individuals it was difficult to determine the cortical and trabecular bone interface. As noted in our results, we observed differences in the lateral and medial regions that were difficult to quantify because there are not appropriate anatomical landmarks to demarcate these regions and there is gross morphological variability between species and individuals. This is a limitation common to all trabecular bone studies and is best addressed through acknowledgement, transparency, and a description of the variability. We used a standard method of outlining trabecular regions, as described in our methods, to help cope with this limitation.

ACKNOWLEDGEMENTS

Mitra Bolouri, DDS, and Allen Mortimer, DDS helped extract the human zygoma samples and Leticia Castenada helped with the microCT analysis. The authors appreciate the aid of Tim Ryan, Richard Ketcham, and Ian Grosse, who have provided expert advice on more than one occasion. We would like to thank the Southwest National Primate Center and the Yerkes National Primate Research Center at Emory University in Atlanta, Georgia for providing the *Pan troglodytes* specimens. Thank you to the Wild Animal Park Planckendael (Muizen, Belgium) and the Royal Zoological Society of Antwerp for providing the bonobo specimen and Dr. Francis Vercammen and Maj Deckx for the transporting of this specimen, and Dr. Kris D'Aout for facilitating access. Thank you to Dr. Andrew F. McIntosh for helping to edit this manuscript. The authors also appreciate the helpful feedback given by the reviewers.

REFERNCES

Aaron JE, Makins NB, Sagreiya K. 1987. The microanatomy of trabecular bone loss in normal aging men and women. Clin Orthop Relat Res 260–271.

Ashman RB, Rho JY, Turner CH. 1989. Anatomical variation of orthotropic elastic moduli of the proximal human tibia. J Biomech 22:895–900.

Biewener AA, Fazzalari NL, Konieczynski DD, Baudinette RV. 1996. Adaptive changes in trabecular architecture in relation to functional strain patterns and disuse. Bone 19:1–8.

Carrier DH, and Morgan MH. 2015. Protective buttressing of the hominin face. Biol Rev 90:330–346.

Cartmill M. 1970. The Orbits of Arboreal Mammals: A Reassessment of the Arboreal Theory of Primate Evolution. Chicago: University of Chicago.

Chalk J, Richmond BG, Ross CF, Strait DS, Wright BW, Spencer MA, Wang Q, Dechow PC. 2011. A finite element analysis of masticatory stress hypotheses. Am J Phys Anthropol 145:1–10.

Chirchir H, Kivell TL, Ruff CB, Hublin JJ, Carlson KJ, Zipfel B, Richmond BG. 2015. Recent origin of low trabecular bone density in modern humans. Proc Natl Acad Sci USA 112:366–371.

Cotter MM, Simpson SW, Latimer BM, Hernandez CJ. 2009. Trabecular microarchitecture of hominoid thoracic vertebrae. Anat Rec 292:1098–1106.

Dechow PC, Hylander WL. 2000. Elastic properties and masticatory bone stress in the macaque mandible. Am J Phys Anthropol 112:553–574.

Ding M, Odgaard A, Hvid I. 2003. Changes in the three-dimensional microstructure of human tibial cancellous bone in early osteoarthritis. J Bone Joint Surg Br 85:906–912.

Dzialo C, Wood SA, Berthaume M, Smith A, Dumont ER, Benazzi S, Weber GW, Strait DS, Grosse IR. 2014. Functional implications of squamosal suture size in *Paranthropus boisei*. Am J Phys Anthropol 153:260–268.

Endo B. 1966. Experimental studies on the mechanical significance of the form of the human facial skeleton. J Faculty Sci 3:5–106.

Endo B. 1970. Analysis of stresses around the orbit due to masseter and temporalis muscles respectively. J Anthropol Soc Nippon 78: 251–266.

Endo B. 1973. Stress analysis on the facial skeleton of gorilla by means of wire strain gauge method. Primates 14:37–45.

Fajardo RJ, Muller R. 2001. Three-dimensional analysis of nonhuman primate trabecular architecture using micro-computed tomography. Am J Phys Anthropol 115:327–336.

Fajardo RJ, Muller R, Ketcham RA, Colbert M. 2007. Nonhuman anthropoid primate femoral neck trabecular architecture and its relationship to locomotor mode. Anat Rec 290:422–436.

Gharpure P, Kontogiorgos ED, Opperman LA, Ross CF, Strait DS, Smith A, Pryor LC, Wang Q, Dechow PC. Elastic properties of chimpanzee craniofacial cortical bone. Anat Rec 299:1718–1733.

Giesen EB, Ding M, Dalstra M, van Eijden TM. 2001. Mechanical properties of cancellous bone in the human mandibular condyle are anisotropic. J Biomech 34:799–803.

Giesen EBW, Ding M, Dalstra M, van Eijden TMGJ. 2004. Changed morphology and mechanical properties of cancellous bone in the mandibular condyles of edentate people. J Dent Res 83:255–259.

Giesen EBW, van Eijden TMGJ. 2000. The three-dimensional cancellous bone architecture of the human mandibular condyle. J Dent Res 79:957–963.

Goldstein SA, Goulet R, McCubbrey D. 1993. Measurement and significance of three-dimensional architecture to the mechanical integrity of trabecular bone. Calcif Tissue Int 53: S127–S132. discussion S132-123.

Griffin NL, D'Aout K, Ryan TM, Richmond BG, Ketcham RA, Postnov A. 2010. Comparative forefoot trabecular bone architecture in extant hominids. J Hum Evol 59:202–213.

Groning F, Liu J, Fagan MJ, O'Higgins P. 2011. Why do humans have chins? Testing the mechanical significance of modern human symphyseal morphology with finite element analysis. Am J Phys Anthropol 144:593–606.

Harrigan TP, Mann RW. 1984. Characterization of microstructural anisotropy in orthotropic materials. J Mater Sci 19:761–767.

Hildebrand T, Laib A, Muller R, Dequeker J, Ruegsegger P. 1999. Direct three-dimensional morphometric analysis of human cancellous bone: microstructural data from spine, femur, iliac crest, and calcaneus. J Bone Miner Res 14:1167–1174.

Hildebrand T, Rüegsegger P. 1997. A new method for the model-independent assessment of thickness in three-dimensional images. J Microsc-Oxford 185:67–75.

Kneissel M, Boyde A, Hahn M, Teschler-Nicola M, Kalchhauser G, Plenk H Jr. 1994. Age- and sex-dependent cancellous bone changes in a 4000y BP population. Bone 15:539–545.

Kupczik K, Dobson CA, Crompton RH, Phillips R, Oxnard CE, Fagan MJ, O'Higgins P. 2009. Masticatory loading and bone

adaptation in the supraorbital torus of developing macaques. Am J Phys Anthropol 139:193–203.
Kupczik K, Dobson CA, Fagan MJ, Crompton RH, Oxnard CE, O'Higgins P. 2007. Assessing mechanical function of the zygomatic region in macaques: validation and sensitivity testing of finite element models. J Anat 210:41–53.
Lanyon LE. 1973. Analysis of surface bone strain in the calcaneus of sheep during normal locomotion. J Biomech 6:41–49.
Lanyon LE. 1974. Experimental support for trajectorial theory of bone structure. J Bone Joint Surg Br B 56:160–166.
Ledogar J, Smith A, Benazzi S, Weber G, Spencer M, Carlson K, McNulty K, Dechow P, Grosse I, Ross C, et al. 2016. Mechanical evidence that *Australopithecus sediba* was limited in its ability to eat hard foods. Nat Commun 2016;7:10596.
Lieberman D. 2011. The Evolution of the Human Head. Cambridge, MA: Belknap Press of Harvard University Press.
Lorensen WE, Cline HE. 1987. Marching cubes: A high resolution 3D surface construction algorithm. In: Proceedings of the 14th Annual Conference on Computer Graphics and Interactive Techniques: ACM New York, NY. p 163–169.
Lublinsky S, Ozcivici E, Judex S. 2007. An automated algorithm to detect the trabecular-cortical bone interface in micro-computed tomographic images. Calcif Tissue Int 81:285–293.
Maga M, Kappelman J, Ryan TM, Ketcham RA. 2006. Preliminary observations on the calcaneal trabecular microarchitecture of extant large-bodied hominoids. Am J Phys Anthropol 129:410–417.
Odgaard A, Gundersen HJG. 1993. Quantification of connectivity in cancellous bone, with special emphasis on 3-D reconstructions. Bone 14:173–182.
Pontzer H, Lieberman DE, Momin E, Devlin MJ, Polk JD, Hallgrimsson B, Cooper DM. 2006. Trabecular bone in the bird knee responds with high sensitivity to changes in load orientation. J Exp Biol 209:57–65.
Pryor LC. 2015. Trabecular Bone Structure and Cellular Morphology in the Primate Craniofacial Skeleton. PhD Thesis. Department of Biomedical Sciences, Texas A&M University. 197.
Rak Y. 1983. The Australopithecine Face. New York: Academic Press.
Richmond BG, Wright BW, Grosse I, Dechow PC, Ross CF, Spencer MA, Strait DS. 2005. Finite element analysis in functional morphology. Anat Rec A Discov Mol Cell Evol Bio 283:259–274.
Ridler TW, Calvard S. 1978. Picture thresholding using an iterative selection method. IEEE T Syst Man Cyb 8:630–632.
Ross CF. 1995. Muscular and osseous anatomy of the primate anterior temporal fossa and the functions of the postorbital septum. Am J Phys Anthropol 98:275–306.
Ross CF, Berthaume MA, Dechow PC, Iriarte-Diaz J, Porro LB, Richmond BG, Spencer M, Strait D. 2011. In vivo bone strain and finite-element modeling of the craniofacial haft in catarrhine primates. J Anat 218:112–141.
Ross CF, Hylander WL. 1996. In vivo and in vitro bone strain in the owl monkey circumorbital region and the function of the postorbital septum. Am J Phys Anthropol 101:183–215.
Ross CF, Wall CE. 2000. Mammalian feeding and primate evolution: An overview. Am J Phys Anthropol 112:449–453.
Ryan T, Ketcham R. 2002a. Analysis of trabecular bone structure in the femoral heads of two Omomyid primates. Am J Phys Anthropol 135–135.
Ryan T, Shaw C. 2013. Trabecular bone microstructure scales allometrically in the primate humerus and femur. Proc R Soc B 280:
Ryan TM, Colbert M, Ketcham RA, Vinyard CJ. 2010a. Trabecular bone structure in the mandibular condyles of gouging and non-gouging platyrrhine primates. Am J Phys Anthropol 141:583–593.
Ryan TM, Ketcham RA. 2002b. Femoral head trabecular bone structure in two omomyid primates. J Hum Evol 43:241–263.
Ryan TM, Ketcham RA. 2002c. The three-dimensional structure of trabecular bone in the femoral head of strepsirrhine primates. J Hum Evol 43:1–26.
Ryan TM, Krovitz GE. 2006. Trabecular bone ontogeny in the human proximal femur. J Hum Evol 51:591–602.
Ryan TM, Shaw CN. 2012. Unique suites of trabecular bone features characterize locomotor behavior in human and non-human anthropoid primates. Plos One 7:e41037.
Ryan TM, van Rietbergen B. 2005. Mechanical significance of femoral head trabecular bone structure in *Loris* and *Galago* evaluated using micromechanical finite element models. Am J Phys Anthropol 126:82–96.
Ryan TM, Walker A. 2010. Trabecular bone structure in the humeral and femoral heads of Anthropoid primates. Anat Rec 293:719–729.
Smith AL, Benazzi S, Ledogar JA, Tamvada K, Pryor Smith LC, Weber GW, Spencer MA, Dechow PC, Grosse IR, Ross CF, et al. 2015a. Biomechanical implications of intraspecific shape variation in chimpanzee crania: moving toward an integration of geometric morphometrics and finite element analysis. Anat Rec 298:122–144.
Smith AL, Benazzi S, Ledogar JA, Tamvada K, Pryor Smith LC, Weber GW, Spencer MA, Lucas PW, Michael S, Shekeban A, et al. 2015b. The feeding biomechanics and dietary ecology of *Paranthropus boisei*. Anat Rec 298:145–167.
Smith RJ, Jungers WL. 1997. Body mass in comparative primatology. J Hum Evol 32:523–559.
Strait DS, Wang Q, Dechow PC, Ross CF, Richmond BG, Spencer MA, Patel BA. 2005. Modeling elastic properties in finite-element analysis: How much precision is needed to produce an accurate model?. Anat Rec 283A:275–287.
Strait DS, Grosse IR, Dechow PC, Smith AL, Wang Q, Weber GW, Neubauer S, Slice DE, Chalk J, Richmond BG, et al. 2010. The structural rigidity of the cranium of *Australopithecus africanus*: implications for diet, dietary adaptations, and the allometry of feeding biomechanics. Anat Rec 293:583–593.
Strait DS, Richmond BG, Spencer MA, Ross CF, Dechow PC, Wood BA. 2007. Masticatory biomechanics and its relevance to early hominid phylogeny: An examination of palatal thickness using finite-element analysis. J Hum Evol 52:585–599.
Strait DS, Weber GW, Neubauer S, Chalk J, Richmond BG, Lucas PW, Spencer MA, Schrein C, Dechow PC, Ross CF, et al. 2009. The feeding biomechanics and dietary ecology of *Australopithecus africanus*. Proc Natl Acad Sci USA 106:2124–2129.
Trussell HJ. 1979. Picture thresholding using an iterative selection method - comments. IEEE T Syst Man Cyb 9:311–311.
van Ruijven LJ, Giesen EBW, Mulder L, Farella A, van Eijden TMGJ. 2005. The effect of bone loss on rod-like and plate-like trabeculae in the cancellous bone of the mandibular condyle. Bone 36:1078–1085.
van Ruijven LJ, Giesen EBW, van Eijden TMGJ. 2002. Mechanical significance of the trabecular microstructure of the human mandibular condyle. J Dent Res 81:706–710.
Wang Q and Dechow PC. 2006. Elastic properties of external cortical bone in the craniofacial skeleton of the rhesus monkey. Am J Phys Anthropol 131:402–415.
Wang Q, Wood SA, Grosse IR, Ross CF, Zapata U, Byron CD, Wright BW, Strait DS. 2012. The role of the sutures in biomechanical dynamic simulation of a macaque cranial finite element model: Implications for the evolution of craniofacial form. Anat Rec 295:278–288.
Whitehouse WJ. 1974. Quantitative morphology of anisotropic trabecular bone. J Microsc 101:153–168.
Zar JH. 1999. Biostatistical Analysis. 4th ed.Upper Saddle River, NJ: Prentice Hall.